Relationship between $\%dd(10)_x$ and stopping-power ratios for flattening filter free accelerators: A Monte Carlo study

Guoming Xiong[a] and D. W. O. Rogers
Physics Department, Carleton University, Ottawa, Ontario, K1S 5B6 Canada

(Received 31 December 2007; revised 26 February 2008; accepted for publication 11 March 2008; published 28 April 2008)

The relationship between the photon beam quality specifier $\%dd(10)_x$ and the Spencer–Attix water to air restricted mass collision stopping-power ratio, $(\bar{L}/\rho)_{\text{air}}^{\text{water}}$, is studied using Monte Carlo simulation with realistic beams in contrast to the previously used realistic but uniform spectra from an isotropic point source. The differences between accelerators with and without flattening filters are investigated since flattening filter free accelerators appear to be useful for IMRT. Our results show that the standard relationship between $\%dd(10)_x$ and $(\bar{L}/\rho)_{\text{air}}^{\text{water}}$, which is used in the TG–51 protocol to calculate the quality conversion factor k_Q, is acceptable for beams with or without a flattening filter with a maximum error of 0.4%, although a fit to the new data would reduce the maximum error to 0.2%. Reasons for differences between the individual values of $\%dd(10)_x$ and $(\bar{L}/\rho)_{\text{air}}^{\text{water}}$ with and without a flattening filter are studied. Specifically the differences due to the softening of the beam, the change in shape of the profile, and the inclusion of radial variations in the photon energy spectra, are investigated. It is shown that if TPR_{10}^{20} is used as a beam quality specifier, there are two different relationships between TPR_{10}^{20} and $(\bar{L}/\rho)_{\text{air}}^{\text{water}}$ which differ by 0.4%–1%. When using TPR_{10}^{20} as a beam quality specifier in a beam without a flattening filter, one should subtract 0.5% from the value of k_Q for a given value of TPR_{10}^{20}. [DOI: 10.1118/1.2905028]

Key words: beam quality specifier, photon beams, stopping-power ratios, $\%dd(10)_x$, $\text{TPR}_{10}{}^{20}$ Monte Carlo, flattening filter free

I. INTRODUCTION

The photon beam quality specifier in the AAPM's TG-51 dosimetry protocol[1] is $\%dd(10)_x$, which is the photon component of the percentage depth dose on the central axis at 10 cm depth for a $10\times10\ \text{cm}^2$ field size on the surface of a phantom at an SSD of 100 cm. The value of $\%dd(10)_x$ has been shown to be an ideal quantity to specify the quality of accelerator photon beams[2] because $\%dd(10)_x$ corresponds uniquely to the Spencer–Attix water to air restricted stopping-power ratio, $(\bar{L}/\rho)_{\text{air}}^{\text{water}}$ at the reference depth in photon beams and because it remains sensitive to the beam quality at high energies. Furthermore, for high-energy clinical photon beams (energies above 4 MV) there is a linear relationship between $\%dd(10)_x$ and $(\bar{L}/\rho)_{\text{air}}^{\text{water}}$. The value of $(\bar{L}/\rho)_{\text{air}}^{\text{water}}$ is the major component of the variation of the beam quality conversion factor, k_Q, used in the TG-51 protocol. Based on Monte Carlo simulations the linear relationship used in TG-51 is:[3]

$$\left(\frac{\bar{L}}{\rho}\right)_{\text{air}}^{\text{water}} = 1.275 - 0.00231(\%dd(10)_x)\,. \qquad (\text{TG}-51) \quad (1)$$

This relationship was derived using the photon energy spectra from many linear accelerators. The incident beams were assumed to be uniform in energy spectrum and fluence across the field. This relationship is known to be acceptable for accelerators equipped with a flattening filter—a device designed to produce a uniform dose profile across the field at some depth, often 10 cm. However, use of a flattening filter may be unnecessary when doing intensity modulated radiation therapy (IMRT). For IMRT applications the incident fluence of the field on the patient can be controlled by the multileaf collimator whether the initial field is flat or not. It has been reported that removing the flattening filter provides some advantages, such as faster treatment and smaller out-of-field doses to the patient.[4–8] Therefore the flattening filter may no longer be required for IMRT related treatments and machines without the flattening filter may become common. TomoTherapy[9] is a practical example of this kind of machine which is already widely used.

Removing the flattening filter leads to changes in the energy spectrum and the lateral profile of the fluence on a patient or a phantom. These changes cause some fundamental differences in the physical properties of the beam as compared to those in traditional therapy applications and these have been studied both experimentally and numerically.[4,7,8,10–12] However, the effect on the relationship between $\%dd(10)_x$ and $(\bar{L}/\rho)_{\text{air}}^{\text{water}}$ due to the removal of the flattening filter has not been investigated. As this relationship is fundamentally important in clinical reference dosimetry, we have conducted an investigation to address this particular subject using Monte Carlo techniques. This study does not apply to Tomotherapy machines since they cannot produce a $10\times10\ \text{cm}^2$ field at an SSD of 100 cm and reference dosimetry must be handled differently.[13,14] In addition, previous studies related to the relationship between $\%dd(10)_x$ and

$(\bar{L}/\rho)^{\text{water}}_{\text{air}}$ were done using photon spectra which were assumed to be uniform on the phantom surface in terms of fluence and energy spectrum.[2,3,15] In this study calculations are done using more realistic beams from the accelerators which take into account spectral and fluence variations on the surface of the water phantom.

II. METHODS

II.A. Accelerator models

Nine photon beams from three major manufacturers of medical linear accelerators are simulated using BEAMnrc/EGSnrc[16–18] and the same geometry specifications as used previously.[19,20] Improved models are not investigated since the details of each beam are not critical to this study. However, estimates of the energy and intensity distributions of the incident electron beams must be redetermined because of the differences between EGSnrc and EGS4. We used the same methods and experimental data as Sheikh-Bagheri and Rogers.[19] The other difference in the simulations is that directional bremsstrahlung splitting[21] instead of selective bremsstrahlung splitting is used in BEAMnrc to improve the efficiency. In the process of determining the energy and intensity distributions of the incident electron beams the accelerators are equipped with a flattening filter because the measured data, such as average depth-dose curves and off-axis factors,[22] were based on accelerators with a flattening filter. In general we found that the incident electron energies with EGSnrc are slightly less than they are with EGS4 and the full width at half maximum of the incident beams varied by as much as ± 1 mm.

II.B. Calculation of $\%dd(10)_x$ and $(\bar{L}/\rho)^{\text{water}}_{\text{air}}$

This study concerns the relationship between $\%dd(10)_x$ and the Spencer–Attix restricted mass collision stopping power ratios, $(\bar{L}/\rho)^{\text{water}}_{\text{air}}$ under reference conditions in the flattening filter free (FFF) case as well as the case with flattening filter (WFF). We consider three methods to calculate $\%dd(10)_x$ and $(\bar{L}/\rho)^{\text{water}}_{\text{air}}$:

1. Calculate $\%dd(10)_x$ directly using BEAMnrc with a water phantom starting at an SSD of 100 cm and record the phase-space file on the plane at the same SSD. A second calculation uses the phase-space file to calculate the value of $(\bar{L}/\rho)^{\text{water}}_{\text{air}}$ using the user-code SPRRZnrc;[23]
2. Record the phase-space file at SSD=100 cm using BEAMnrc and then calculate $\%dd(10)_x$ using DOSRZnrc and $(\bar{L}/\rho)^{\text{water}}_{\text{air}}$ using SPRRZnrc;
3. Record the phase-space file at SSD=100 cm using BEAMnrc, obtain the energy spectrum averaged over the entire 10×10 cm^2 field and the radial distribution of the photon beam from the phase-space file, and then use the spectrum and the radial distribution as the incident source with DOSRZnrc and SPRRZnrc to calculate $\%dd(10)_x$ and $(\bar{L}/\rho)^{\text{water}}_{\text{air}}$, respectively.

The first two methods are equivalent, whereas method 3 introduces several approximations. In particular it ignores the variation in the spectrum across the field. In this work we use method 1 to obtain the relationship between the two quantities (see Sec. III A below), and use method 3 to investigate the effects on $\%dd(10)_x$ and $(\bar{L}/\rho)^{\text{water}}_{\text{air}}$ caused by the presence or absence of the flattening filter (see Sec. III B below).

The scoring region used to calculate $\%dd(10)_x$ and $(\bar{L}/\rho)^{\text{water}}_{\text{air}}$ is a column with a radius of 1 cm along the central axis of the phantom. Despite using the cylindrically symmetric codes DOSRZnrc and SPRRZnrc, when a phase space file is used as input, the full three-dimensional geometry is in effect because we only do the calculations on the central axis. In order to get the maximum dose accurately, the thickness of the depth bins for the $\%dd(10)_x$ calculation is 0.2 cm in the buildup region to a depth of 4 cm and is 0.5 cm to a depth larger than 10 cm. The bin size for the $(\bar{L}/\rho)^{\text{water}}_{\text{air}}$ calculation is 0.5 cm at all depths since the buildup region does not have a special meaning for the calculation. The option in BEAMnrc and DOSRZnrc, which allows one to score separately the dose from photons (or electrons), is used to calculate the photon component of the percentage depth-dose curve which gives $\%dd(10)_x$.

The SPRRZnrc and DOSRZnrc user-codes of the EGSnrc system were modified to allow use of a source from which the incident particles are coming from a single point with a spectrum and a radial distribution on the phantom surface. This allows an investigation of the effects of the realistic radial distribution (with horns or central peak) versus the previously assumed flat distributions. This approach approximates a square field by a circular field with an appropriate radial distribution.

In the simulations using BEAMnrc and DOSRZnrc, default transport settings and electron range rejection are used. The energy thresholds for electron and photon production and transportation (AE=ECUT, AP=PCUT) are set to be 700 and 1 keV (total energy), respectively. However, when calculating $(\bar{L}/\rho)^{\text{water}}_{\text{air}}$ using SPRRZnrc, the electron thresholds are 521 keV and no range rejection is used.

III. RESULTS AND DISCUSSION

III.A. Effects of removing flattening filter on $\%dd(10)_x$ versus $(\bar{L}/\rho)^{\text{water}}_{\text{air}}$

The values of $\%dd(10)_x$ and $(\bar{L}/\rho)^{\text{water}}_{\text{air}}$ calculated using method 1 simulations, both WFF and FFF, are given in Table I and shown in Fig 1. The relationship used by TG-51[3] is shown (solid line) for comparison[24,3] [i.e., above $\%dd(10)_x$ =63.35% Eq. (1) applies, below this value a linear interpolation to the stopping-power ratio of ^{60}Co (i.e., 1.1337) applies, and for $\%dd(10)_x$ below 58.4% the value of $(\bar{L}/\rho)^{\text{water}}_{\text{air}}$ is constant at the ^{60}Co value]. Figure 1 shows that for all WFF beams, the data are in good agreement with TG-51's values, although most of the data points are on or slightly above the TG-51 values. For the nine WFF beams the root

TABLE I. Comparison between values of $\%dd(10)_x$ and $(\bar{L}/\rho)^{water}_{air}$ calculated using method 1 and method 3. For method 1, the $\%dd(10)_x$ calculation is done by a BEAMnrc simulation and the $(\bar{L}/\rho)^{water}_{air}$ calculation with a phase-space file from the same BEAMnrc calculation. Method 3 uses spectral and radial distributions obtained from phase-space files recorded in BEAMnrc simulations and assuming uniform spectra from a point source at a SSD of 100 cm. For $\%dd(10)_x$ the statistical uncertainties are smaller than 0.1% and for $(\bar{L}/\rho)^{water}_{air}$ the statistical uncertainties are smaller than 0.01%. The most accurate values are those calculated using method 1 with the full beam simulations.

	With flattening filter (WFF)				Flattening filter free (FFF)			
	Method 1		Method 3		Method 1		Method 3	
Beam	$\%dd(10)_x$	$(\bar{L}/\rho)^{water}_{air}$	$\%dd(10)_x$	$(\bar{L}/\rho)^{water}_{air}$	$\%dd(10)_x$	$(\bar{L}/\rho)^{water}_{air}$	$\%dd(10)_x$	$(\bar{L}/\rho)^{water}_{air}$
Varian 4 MV	62.12	1.1293	61.89	1.1293	58.29	1.1313	57.88	1.1313
Varian 6 MV	66.63	1.1211	66.22	1.1214	63.37	1.1240	63.03	1.1240
Varian 10 MV	74.18	1.1054	73.44	1.1069	69.49	1.1120	69.22	1.1120
Varian 15 MV	77.19	1.0998	76.68	1.1005	74.80	1.1018	74.46	1.1019
Varian 18 MV	80.13	1.0925	79.56	1.0933	77.45	1.0959	77.12	1.0959
KD2 6 MV	66.78	1.1201	66.49	1.1203	64.38	1.1224	63.91	1.1224
KD2 18 MV	77.71	1.0969	76.60	1.0990	73.91	1.1034	73.71	1.1035
SL25 6 MV	67.99	1.1191	67.31	1.1195	64.89	1.1219	64.68	1.1220
SL25 25 MV	83.16	1.0830	82.30	1.0852	80.82	1.0878	80.43	1.0878

mean square deviation (RMSD) about the TG-51 line is 0.0016 with the largest deviation (0.0028) being for the Varian 15 MV beam. In the fit used by TG-51, the RMSD was 0.0011 for 22 beams.[3] The slightly larger RMSD in this work may be due to using realistic models of the accelerators. The radial distribution of the incident fluence is not completely flat as assumed previously (see Fig. 4 below), and different beams may have different lateral dose profiles as the flattening filters for different beams are not the same.

For the FFF beams at higher energies (above 10 MV), the relationship described by Eq. (1) is still followed although the data points are systematically slightly below the TG-51 line; for beams below 10 MV the deviations are somewhat larger. The RMSD about the TG-51 values is 0.0030 with the maximum deviation being for the Varian 6 MV beam (0.0041). These results show that the linear relationship between $\%dd(10)_x$ and $(\bar{L}/\rho)^{water}_{air}$ still exists for FFF beams, and the somewhat larger RMSD compared with that of the WFF beams suggests that Eq. (1) is no longer the best linear fit when including the FFF beams. A new fit including all 17 beams with $\%dd(10)_x > 62.0\%$ is shown as a dashed line in Fig. 1. The data point of the lowest energy beam (FFF, Varian 4 MV), is excluded as it is below the range of the linear relationship. The new relationship between $\%dd(10)_x$ and $(\bar{L}/\rho)^{water}_{air}$ is:

$$\left(\frac{\bar{L}}{\rho}\right)^{water}_{air} = 1.258 - 0.00209(\%dd(10)_x) . \quad \text{(universal)} \tag{2}$$

The RMSD for all beams about Eq. (2) is 0.0016 which is the same as the RMSD of WFF beams about Eq. (1). The largest deviation is from the Varian 15 MV beam (0.0022), but is smaller than the maximum deviation of the WFF beams about the TG-51 values (0.0028).

In summary, when the FFF beams are considered there is a slight change in the relationship between $\%dd(10)_x$ and $(\bar{L}/\rho)^{water}_{air}$ but the changes are not significant enough to justify distinguishing between the two cases. A unique relationship between $\%dd(10)_x$ and $(\bar{L}/\rho)^{water}_{air}$ still exists and is linear, although this latter point is not critical.

To see how the change in relationship from Eq. (1) to Eq. (2) affects the values of k_Q in the TG-51 dosimetry protocol,[1] Fig. 2 shows the calculated k_Q values as a function of the $\%dd(10)_x$ for a cylindrical Farmer-like chamber, namely an NE2571 chamber, based on both Eq. (1) and Eq. (2). As in the TG-51 case, we adopted a linear interpolation between

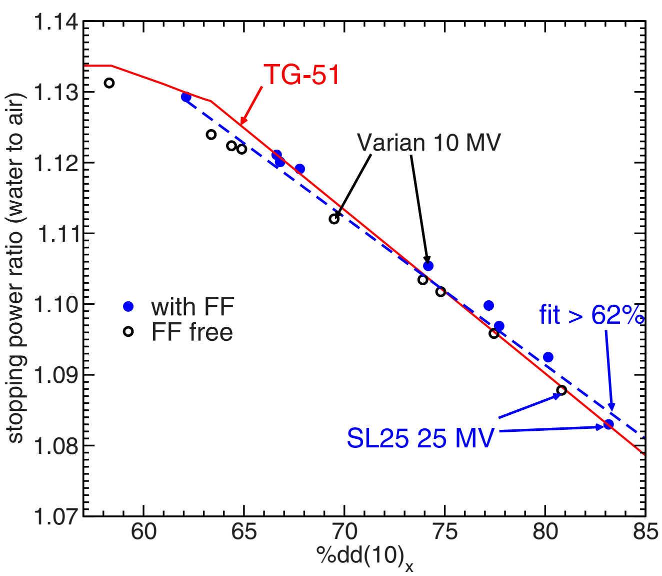

FIG. 1. Values of $\%dd(10)_x$ and Spencer–Attix mass restricted collision water to air stopping power ratios, $(\bar{L}/\rho)^{water}_{air}$, calculated using full accelerator simulations for cases with (WFF) or without (FFF) flattening filters. The solid line shows the values used in the AAPM's TG-51 protocol (Ref. 1) and the dashed line shows a best fit to all the present data with $\%dd(10)_x > 62\%$.

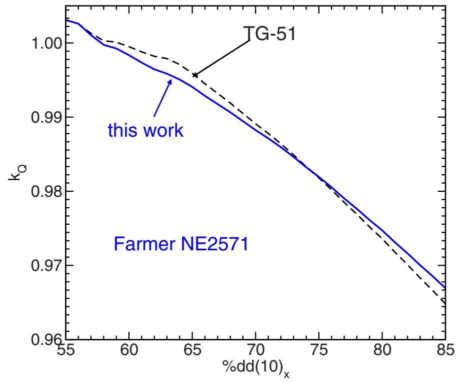

FIG. 2. Values of k_Q for an NE2571 Farmer-like chamber calculated using different relationships between $\%dd(10)_x$ and the $(\bar{L}/\rho)^{\text{water}}_{\text{air}}$. Dashed line: calculations with the relationship used in TG-51, i.e., Eq. (1); thick solid line—calculations with the present relationship, i.e., Eq. (2).

62% and ^{60}Co value. The maximum difference between the two calculations is only about 0.2%. A detailed description of k_Q calculations can be found in Ref. 24.

III.B. Changes in $\%dd(10)_x$ and $(\bar{L}/\rho)^{\text{water}}_{\text{air}}$

When FFF beams are involved, as seen above, the relationship between beam quality specifier $\%dd(10)_x$ and $(\bar{L}/\rho)^{\text{water}}_{\text{air}}$ has only changed slightly. However, for beams with the same nominal accelerating potential the individual values of $\%dd(10)_x$ and $(\bar{L}/\rho)^{\text{water}}_{\text{air}}$ have changed considerably. Figure 1 shows that the FFF values of $\%dd(10)_x$ are systematically "lower" than WFF values while the values of $(\bar{L}/\rho)^{\text{water}}_{\text{air}}$ are slightly larger. These different values must come from three fundamental changes in the photon beams caused by removing the flattening filter, i.e., a softer energy spectrum, a more uniform spectrum across the field, and a non-flat lateral profile of the incident fluence. All of these changes will affect the values of $\%dd(10)_x$ and $(\bar{L}/\rho)^{\text{water}}_{\text{air}}$, but they play different roles. In the remainder of this section we investigate what are the effects of each of these changes.

In Fig. 3 the values of $\%dd(10)_x$ and $(\bar{L}/\rho)^{\text{water}}_{\text{air}}$ are calculated using spectra determined from the phase-space files but under the assumption that the spectra are the same across the beam and the beam profiles from the point source are also assumed to be uniform across the beam. These calculations correspond to those used to generate the values in TG-51.[3] This comparison emphasizes the effects of the change in the spectra when the flattening filter is removed. Since the spectrum becomes softer, the value of $\%dd(10)_x$ decreases between 1.5% to 5% of its value (e.g., $\%dd(10)_x$ decreases from 73.4% to 69.9%=5%). Likewise, the softer spectrum means that the value of $(\bar{L}/\rho)^{\text{water}}_{\text{air}}$ increases by 0.3%–0.7%. However, there is still a linear relationship between $\%dd(10)_x$ and $(\bar{L}/\rho)^{\text{water}}_{\text{air}}$ and the fit shown in Fig. 3 to these data gives an RMSD of 0.0009 with a maximum deviation of 0.0016. This fit is only slightly different from that used in TG-51.

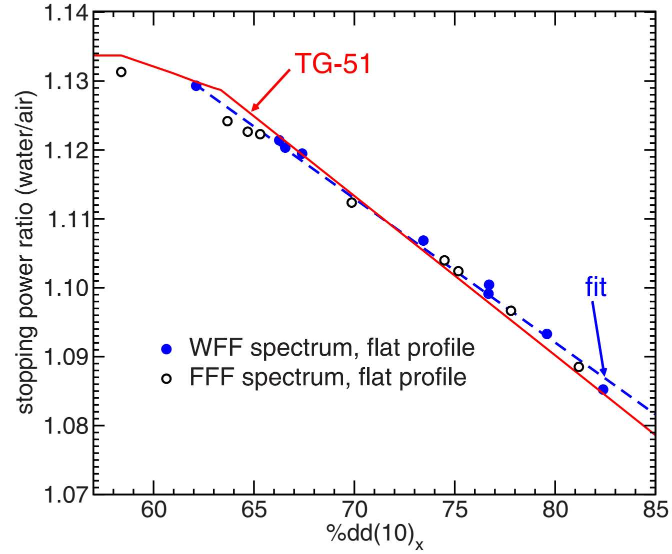

FIG. 3. Values of $\%dd(10)_x$ and $(\bar{L}/\rho)^{\text{water}}_{\text{air}}$ for nine accelerator beams when uniform spectra and flat radial distributions are used for beams with and without flattening filters (WFF, FFF, respectively). These calculations correspond to those used in the TG-51 protocol (Ref. 3) but the fit to the data differs slightly from the TG-51 fit.

Figure 4 shows that for FFF beams the fluence on the phantom surface decreases laterally while for WFF beams it usually increases slightly laterally to give the well known "horns" which help ensure a flat beam at some depth in a water phantom. In addition to this variation in fluence there is a variation in the average energy which decreases laterally for beams with a flattening filter (see Fig. 5 here or Fig. 12 in Ref. 20 for many beams). In contrast, the average energy is relatively constant in the FFF beams.

To demonstrate the effect of the radial variation of the fluence, Fig. 6 compares values of $\%dd(10)_x$ and $(\bar{L}/\rho)^{\text{water}}_{\text{air}}$ for uniform FFF spectra with either flat profiles or realistic profiles. In this case the changes in $(\bar{L}/\rho)^{\text{water}}_{\text{air}}$ values are very small (from 0.01% to 0.06%), but the decrease in the lateral profiles off axis leads to distinct decreases (0.5%–1.0%) in the values of $\%dd(10)_x$. In a similar plot for the WFF spectra

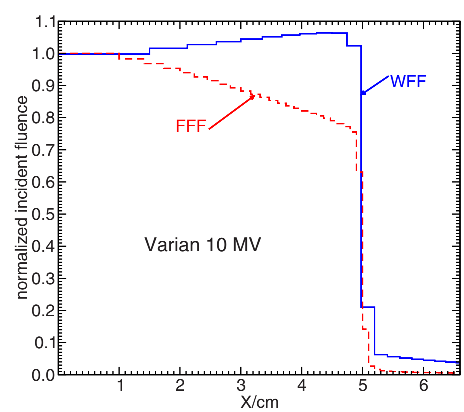

FIG. 4. Radial distribution of the incident fluence for Varian 10 MV FFF (flattening filter free) and WFF (with flattening filter) beams. The distributions are normalized on the central axis.

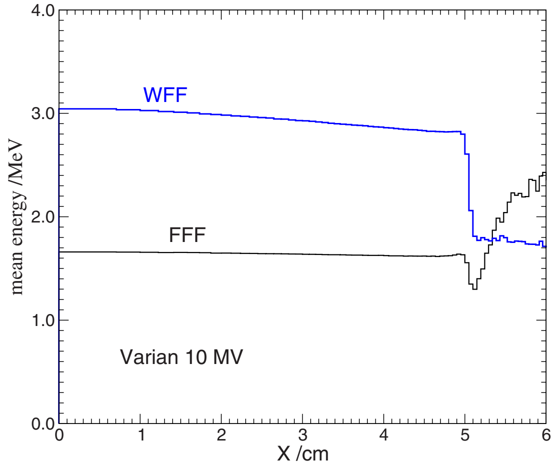

FIG. 5. Mean energy vs radial position for Varian 10 MV FFF (flattening filter free) and WFF (with flattening filter) beams which are 10×10 cm^2. For the FFF case there are very few photons contributing to the average energy outside the field and the few photons getting through the jaw experience significant beam hardening and represent a large component of the fluence.

(not shown) the values of both $(\bar{L}/\rho)^{\text{water}}_{\text{air}}$ and %$dd(10)_x$ are the same within statistical uncertainties whether a realistic radial profile or a flat profile is used. We expected that the realistic profile would give slightly higher values of %$dd(10)_x$, but the "horns" in the beam profile have no apparent effect on the central-axis depth-dose curve.

The last difference to consider is the effect of the variation of the energy spectrum across the field. In Table I, method 1 calculations include all the variation of the spectrum with position, whereas method 3 calculations do not. The values of $(\bar{L}/\rho)^{\text{water}}_{\text{air}}$ do not change between method 1 and method 3 for the FFF beams because the average energy across the field is almost constant, whereas for the WFF beams the

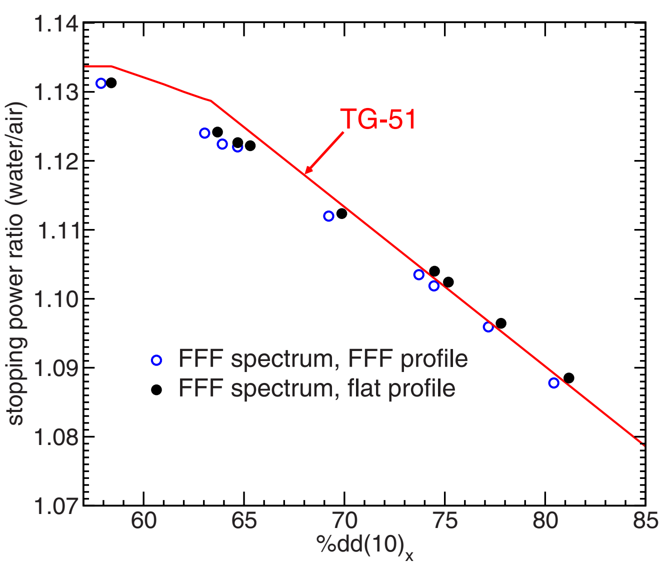

FIG. 6. Values of %$dd(10)_x$ and $(\bar{L}/\rho)^{\text{water}}_{\text{air}}$ for nine accelerator beams when uniform spectra and realistic radial distributions are used for beams without flattening filters (FFF). Solid line: TG-51.

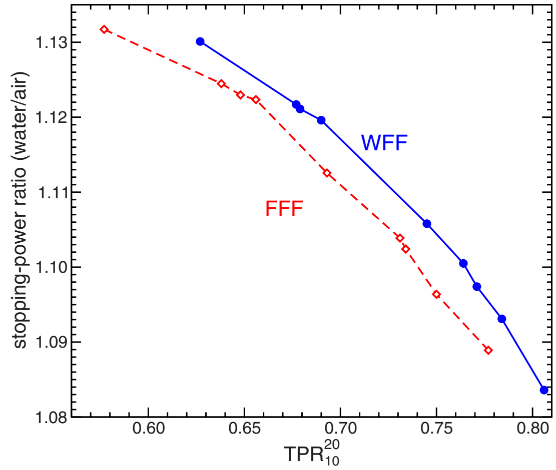

FIG. 7. Relationship between TPR^{20}_{10} and the Spencer–Attix restricted stopping-power ratio for both the WFF and FFF beams.

$(\bar{L}/\rho)^{\text{water}}_{\text{air}}$ values calculated with the constant energy spectra are up to 0.22% higher. These calculations use spectra which are averaged over the entire field and thus, because of the decrease in energy off axis, the spectra near the central axis are softer when using the average spectrum than actually exist on the axis. It is the central axis spectra which most affect the $(\bar{L}/\rho)^{\text{water}}_{\text{air}}$ calculations and thus the softer spectra lead to somewhat higher values of $(\bar{L}/\rho)^{\text{water}}_{\text{air}}$. The situation is not so clear in the case of the value of %$dd(10)_x$ where method 3 values are on average 0.3% lower (absolute difference) than the full simulation values for the FFF beams (for which there is no energy variation across the field) and are on average 0.8% lower for the beams with a flattening filter. The fact that the beams with a flattening filter show a larger decrease in %$dd(10)_x$ in method 3 calculations is consistent with the fact that these calculations use a softer than realistic spectrum on the central axis and thus it is not surprising that the %$dd(10)_x$ value is lower. However, the small difference in the FFF beams is not understood but may reflect the approximation of modeling a square field with a radial distribution.

III.C. Effects of removing flattening filter on TPR^{20}_{10} versus $(\bar{L}/\rho)^{\text{water}}_{\text{air}}$

TPR^{20}_{10} is the beam quality specifier in the TG–21 protocol[25] and in the IAEA's TRS 398 Code of Practice.[26] Thus, the relationship between the value of TPR^{20}_{10} and $(\bar{L}/\rho)^{\text{water}}_{\text{air}}$ for both WFF and FFF beams is of interest. TPR^{20}_{10} values were calculated using two separate calculations with SSDs of 90 and 100 cm and a field size of 10×10 cm^2 at an SAD of 110 cm. The results are shown in Fig. 7. For WFF and FFF beams the TPR^{20}_{10} vs $(\bar{L}/\rho)^{\text{water}}_{\text{air}}$ data form two different curves. For the same value of TPR^{20}_{10}, the differences in $(\bar{L}/\rho)^{\text{water}}_{\text{air}}$ values for FFF vs WFF beam with the same value of TPR^{20}_{10} vary between 0.4% and 1%. Thus if TPR^{20}_{10} is used as the beam quality specifier one must adopt different values of $(\bar{L}/\rho)^{\text{water}}_{\text{air}}$ and hence k_Q values for WFF and FFF beams.

This is not unexpected in the sense that using TPR_{10}^{20} as a beam quality specifier is intended for "clinic-like" photon beams, which, until recently, have always had flattening filters.[15]

IV. CONCLUSIONS

This work uses realistic accelerator models and complete phase-space data for the first time to investigate the relationship between $\%dd(10)_x$ and $(\bar{L}/\rho)_{\mathrm{air}}^{\mathrm{water}}$ and extends the investigation to include clinical accelerators without flattening filters as well as the previously studied clinical accelerators with flattening filters.

The relationship used in the TG-51 protocol[1] is shown to provide reasonable values of k_Q which can be used in beams with or without a flattening filter, with a worst case error of 0.4%. If TG-51 were to be updated, Eq. (2) represents a slightly more accurate relationship between $\%dd(10)_x$ and $(\bar{L}/\rho)_{\mathrm{air}}^{\mathrm{water}}$ which works very well for beams with and without flattening filters. These results have been obtained using detailed accelerator simulations unlike previous investigations,[2,3] thereby accounting for radial variations in fluence and energy spectrum and demonstrating that these factors do not affect the relationship between $\%dd(10)_x$ and $(\bar{L}/\rho)_{\mathrm{air}}^{\mathrm{water}}$.

When the flattening filter is removed, the values of the $\%dd(10)_x$ for a given nominal energy beam decrease considerably because of the softening of the beam even if the beam profile is considered flat (Fig. 3) but also decrease a smaller amount because the beams are not flat (Fig. 6). However, the corresponding increase in $(\bar{L}/\rho)_{\mathrm{air}}^{\mathrm{water}}$ means that the relationship between $\%dd(10)_x$ and $(\bar{L}/\rho)_{\mathrm{air}}^{\mathrm{water}}$ is retained.

For the beam quality specifier, TPR_{10}^{20}, the relationship between TPR_{10}^{20} and $(\bar{L}/\rho)_{\mathrm{air}}^{\mathrm{water}}$ changes by 0.4% to 1% when the clinical accelerators do not have a flattening filter. Thus, when using TPR_{10}^{20} as a beam quality specifier and calibrating a beam without a flattening filter, it is necessary to decrease the value of k_Q by about 0.5% corresponding to the change in $(\bar{L}/\rho)_{\mathrm{air}}^{\mathrm{water}}$.

ACKNOWLEDGMENTS

We wish to thank our colleagues Elsayed Ali, Dan La Russa, Randy Taylor, and Lilie Wang for helpful comments on the manuscript. This work is supported by NSERC, the CRC program, CFI and OIT.

[a]Author to whom correspondence should be addressed. Electronic mail: gxiong@physics.carleton.ca

[1]P. R. Almond, P. J. Biggs, B. M. Coursey, W. F. Hanson, M. S. Huq, R. Nath, and D. W. O. Rogers, "AAPM's TG–51 protocol for clinical reference dosimetry of high-energy photon and electron beams," Med. Phys. **26**, 1847–1870 (1999).
[2]A. Kosunen and D. W. O. Rogers, "Beam quality specification for photon beam dosimetry," Med. Phys. **20**, 1181–1188 (1993).
[3]D. W. O. Rogers and C. L. Yang, "Corrected relationship between $\%dd(10)_x$ and stopping-power ratios," Med. Phys. **26**, 538–540 (1999).
[4]U. Titt, O. N. Vassiliev, F. Ponisch, L. Dong, H. Liu, and R. Mohan, "A flattening filter free photon treatment concept evaluation with Monte Carlo," Med. Phys. **33**, 1595–1602 (2006).
[5]O. N. Vassiliev, U. Titt, S. F. Kry, F. Ponisch, M. T. Gillin, and R. Mohan, "Monte Carlo study of photon fields from a flattening filter-free clinical accelerator," Med. Phys. **33**, 820–827 (2006).
[6]O. N. Vassiliev, U. Titt, F. Pönisch, S. F. Kry, R. Mohan, and M. T. Gillin, "Dosimetric properties of photon beams from a flattening filter free clinical accelerator," Phys. Med. Biol. **51**, 1907–1917 (2006).
[7]U. Titt, O. Vassiliev, F. Pönisch, S. F. Kry, and R. Mohan, "Monte Carlo study of backscatter in a flattening filter-free clinical accelerator," Med. Phys. **33**, 3270–3273 (2006).
[8]F. Pönisch, U. Titt, O. Vassiliev, S. Kry, and R. Mohan, "MCNPX simulation of a multileaf collimator," Med. Phys. **33**, 402–404 (2006).
[9]T. R. Mackie, "History of tomotherapy," Phys. Med. Biol. **51**, R427–R453 (2006).
[10]K. E. Sixel and E. B. Podgorsak, "Buildup region and depth dose maximum of megavoltage x-ray beams," Med. Phys. **21**, 411–416 (1994).
[11]K. Sixel and B. Faddegon, "Calculation of x-ray spectra for radiosurgical beams," Med. Phys. **22**, 1657–1661 (1995).
[12]C. Guillerminet, E. Duverger, R. Gschwind, L. Makovicka, A. Monnier, F. Hamon, and C. David, "Theoretical and experimental study of spectral distortions at theou tput of an accelerator for medical use," Radiat. Phys. Chem. **61**, 611–613 (2001).
[13]S. D. Thomas, M. Mackenzie, D. W. O. Rogers, and B. G. Fallone, "A Monte Carlo derived TG–51 equivalent calibration for helical tomotherapy," Med. Phys. **32**, 1346–1153 (2005).
[14]R. Jeraj, T. R. Mackie, J. Balog, and G. Olivera, "Dose calibration of nonconventional treatment systems applied to helical tomotherapy," Med. Phys. **32**, 570–577 (2005).
[15]N. I. Kalach and D. W. O. Rogers, "Which accelerator photon beams are 'clinic-like' for reference dosimetry purposes?," Med. Phys. **30**, 1546–1555 (2003).
[16]D. W. O. Rogers, B. A. Faddegon, G. X. Ding, C.-M. Ma, J. Wei, and T. R. Mackie, "BEAM: A Monte Carlo code to simulate radiotherapy treatment units," Med. Phys. **22**, 503–524 (1995).
[17]I. Kawrakow and D. W. O. Rogers, "The EGSnrc code system: Monte Carlo simulation of electron and photon transport," Technical Report No. PIRS–701 (4th printing), National Research Council of Canada, Ottawa, Canada, 2003.
[18]D. W. O. Rogers, B. Walters, and I. Kawrakow, "BEAMnrc Users Manual, NRC Technical Report No. PIRS-509(A) rev K," National Research Council of Canada, Ottawa, Canada. http://www.irs.inms.nrc.ca/BEAM/beamhome.html, 2007.
[19]D. Sheikh-Bagheri and D. W. O. Rogers, "Sensitivity of megavoltage photon beam Monte Carlo simulations to electron beam parameters," Med. Phys. **29**, 379–390 (2002).
[20]D. Sheikh-Bagheri and D. W. O. Rogers, "Calculation of nine megavoltage photon beam spectra using the BEAM Monte Carlo code," Med. Phys. **29**, 391–402 (2002).
[21]I. Kawrakow, D. W. O. Rogers, and B. Walters, "Large efficiency improvements in BEAMnrc using directional bremsstrahlung splitting," Med. Phys. **31**, 2883–2898 (2004).
[22]J. A. Purdy, W. Harms, W. F. Hanson, P. Kennedy, T. Kirby, A. Niroomand-Rad, and J. R. Palta, "AAPM RTC TG–46: X-ray beam central axis depth-dose data for use in radiation therapy," [1997 (draft approved by Radiation Therapy Committee)].
[23]D. W. O. Rogers, I. Kawrakow, J. P. Seuntjens, B. R. B. Walters, and E. Mainegra-Hing, "NRC User Codes for EGSnrc," Technical Report No. PIRS–702(RevB), National Research Council of Canada, Ottawa, Canada, 2003.
[24]D. W. O. Rogers, "Fundamentals of dosimetry based on absorbed-dose standards," in *Teletherapy Physics, Present and Future*, edited by J. R. Palta and T. R. Mackie (AAPM, Washington DC, 1996), pp. 319–356.
[25]AAPM TG–21, "A protocol for the determination of absorbed dose from high-energy photon and electron beams," Med. Phys. **10**, 741–771 (1983).
[26]IAEA, *Absorbed Dose Determination in External Beam Radiotherapy: An International Code of Practice for Dosimetry Based on Standards of Absorbed Dose to Water*, volume 398 of Technical Report Series, IAEA, Vienna, 2001.